Arabidopsis nanodomain-delimited ABA signaling pathway regulates the anion channel SLAH3

Fatih Demir[a,1,2], Claudia Horntrich[a,1], Jörg O. Blachutzik[a,b], Sönke Scherzer[a], Yvonne Reinders[c,d,e], Sylwia Kierszniowska[a,f], Waltraud X. Schulze[f,g], Gregory S. Harms[b,3], Rainer Hedrich[a], Dietmar Geiger[a,4], and Ines Kreuzer[a]

[a]Institute for Molecular Plant Physiology and Biophysics, University of Wuerzburg, 97082 Wuerzburg, Germany; [b]Rudolf Virchow Center, University of Wuerzburg, 97080 Wuerzburg, Germany; [c]Institute of Functional Genomics, and [d]Department of Biochemistry I, University of Regensburg, 93053 Regensburg, Germany; [e]Institute for Phamaceutical Biology, University of Wuerzburg, 97082 Wuerzburg, Germany; [f]Max Planck Institute of Molecular Plant Physiology, 14476 Golm, Germany; and [g]Department of Plant Systems Biology, University of Hohenheim, 70593 Stuttgart, Germany

Edited by John Browse, Washington State University, Pullman, WA, and accepted by the Editorial Board February 8, 2013 (received for review July 17, 2012)

The phytohormone abscisic acid (ABA) plays a key role in the plant response to drought stress. Hence, ABA-dependent gene transcription and ion transport is regulated by a variety of protein kinases and phosphatases. However, the nature of the membrane-delimited ABA signal transduction steps remains largely unknown. To gain insight into plasma membrane-bound ABA signaling, we identified sterol-dependent proteins associated with detergent resistant membranes from *Arabidopsis thaliana* mesophyll cells. Among those, we detected the central ABA signaling phosphatase ABI1 (abscisic-acid insensitive 1) and the calcium-dependent protein kinase 21 (CPK21). Using fluorescence microscopy, we found these proteins to localize in membrane nanodomains, as observed by colocalization with the nanodomain marker remorin Arabidopsis thaliana remorin 1.3 (AtRem 1.3). After transient coexpression, CPK21 interacted with SLAH3 [slow anion channel 1 (SLAC1) homolog 3] and activated this anion channel. Upon CPK21 stimulation, SLAH3 exhibited the hallmark properties of S-type anion channels. Coexpression of SLAH3/CPK21 with ABI1, however, prevented proper nanodomain localization of the SLAH3/CPK21 protein complex, and as a result anion channel activation failed. FRET studies revealed enhanced interaction of SLAH3 and CPK21 within the plasma membrane in response to ABA and thus confirmed our initial observations. Interestingly, the ABA-induced SLAH3/CPK21 interaction was modulated by ABI1 and the ABA receptor RCAR1/PYL9 [regulatory components of ABA receptor 1/PYR1 (pyrabactin resistance 1)-like protein 9]. We therefore propose that ABA signaling via inhibition of ABI1 modulates the apparent association of a signaling and transport complex within membrane domains that is necessary for phosphorylation and activation of the S-type anion channel SLAH3 by CPK21.

The phytohormone abscisic acid (ABA) is an important regulator of plant development and stress resistance. ABA regulation of gene expression has been shown to play a crucial role in various biological contexts (1–5). The mechanisms underlying ABA perception and signaling in plant cells have recently been analyzed in great detail, and the essential cytosolic steps of this signaling cascade could be reconstituted in vitro (6). Briefly, four components are sufficient to induce ABA-regulated gene expression in *Arabidopsis* protoplasts. In the default state (*i*), serine-threonine kinases such as open stomata 1 (OST1, also referred to as SnRK2E, SnRK2.6) are kept inactive by the protein phosphatase 2C ABI1 (abscisic-acid insensitive 1). After ABA perception by a cytosolic ABA receptor belonging to the regulatory components of ABA receptor (RCAR)/pyrabactin resistance (PYR)/PYR-like protein (PYL)-family (7, 8), ABI1 phosphatase activity is suppressed (*ii*), leading to OST1 autophosphorylation and thus activation of OST1. Subsequently basic leucine zipper transcription factors, ABRE (ABA-responsive element) binding factors/binding proteins (ABFs/AREBs) (9), are phosphorylated by OST1 (*iii*). Finally, activated ABFs bind to ABA-responsive promoter elements, inducing ABA-regulated gene expression (*iv*). Besides transcriptional regulation, ABA signaling targets membrane components such as ion channels and proton pumps (10, 11).

Three of the four signaling components mentioned above are involved in ABA-induced anion channel activation in the plasma membrane (PM) of guard cells as well (12, 13). Corresponding to the ABA-dependent regulation of transcription factors, ABA perception by RCAR/PYR/PYL receptors causes inactivation of ABI1, release of OST1 from ABI1 inhibition, and activation of the slow anion channel 1 (SLAC1) by phosphorylation (13). Besides OST1, calcium-dependent protein kinases (CPKs) also activate SLAC1 and its homolog SLAH3 in a similar ABA- and ABI1-dependent manner (12, 14, 15). Thus, calcium-independent and -dependent ABA signaling involves both cytosolic and membrane-bound components, and both pathways apparently share the initial steps of signal transduction.

In animal cells, lipid nanodomains, also called "lipid rafts," have been characterized as miniature signaling platforms in the PM (16). In light of a highly dynamic raft concept, such membrane domains have been defined as "dynamic, nanoscale, sterol–sphingolipid-enriched, ordered assemblies of proteins and lipids, in which the metastable raft resting state can be stimulated to coalesce into larger, more stable raft domains by specific lipid–lipid, protein–lipid, and protein–protein oligomerizing interactions" (17). Recently, evidence is emerging that lateral segregation of the PM might play an important role in cell signaling in plants and fungi as well (18, 19).

Results

Plant Detergent-Resistant Membranes Are Enriched in Sterol-Dependent Signaling Proteins. For a long time, membrane domains have often been characterized by their resistance to treatment with mild nonionic detergents like Triton X-100 and thus were referred to as detergent-resistant membranes (DRMs) (20). Albeit detergent treatment leads to artifacts, and presence of a protein in the detergent-resistant fraction does not necessarily imply its in vivo membrane domain association (21, 22), the enrichment of a specific protein in DRMs might suggest an affinity for a distinct lipid

Author contributions: Y.R., W.X.S., G.S.H., R.H., D.G., and I.K. designed research; F.D., C.H., J.O.B., S.S., Y.R., S.K., W.X.S., and I.K. performed research; F.D., C.H., J.O.B., S.S., Y.R., S.K., W.X.S., G.S.H., and I.K. analyzed data; and F.D., Y.R., W.X.S., G.S.H., R.H., D.G., and I.K. wrote the paper.

The authors declare no conflict of interest.

This article is a PNAS Direct Submission. J.B. is a guest editor invited by the Editorial Board.

[1]F.D. and C.H. contributed equally to this work.

[2]Present address: Institute of Neuro- and Sensory Physiology, Medical Faculty, University of Düsseldorf, 40225 Düsseldorf, Germany.

[3]Present address: Department of Biology and Physics, Wilkes University, Wilkes-Barre, PA 18766.

[4]To whom correspondence should be addressed. E-mail: geiger@botanik.uni-wuerzburg.de.

This article contains supporting information online at www.pnas.org/lookup/suppl/doi:10.1073/pnas.1211667110/-/DCSupplemental.

environment and indicate localization in membrane subfractions that correlate to lipid nanodomains (18). Plant DRMs display a clear enrichment in signaling proteins (23–25), but the physiological role of these signaling proteins within DRMs in general and for ABA action in particular is only poorly understood. Therefore, in an initial approach, we isolated DRM fractions from *Arabidopsis thaliana* leaf PM preparations to investigate their protein composition using mass spectrometry. A total of 246 DRM proteins were isolated via treatment with different detergents and digestion protocols (Dataset S1, raw files and search results can be accessed under the dataset identifier: PXD000211 and DOI 10.6019/PXD000211 at the ProteomeXchange database and PRIDE, http://proteomecentral.proteomexchange.org/). As mentioned previously, biochemical preparations of DRMs only reflect a first snapshot of the in vivo protein composition of functional membrane domains (21, 22). To identify proteins depending on a sterol-rich lipid environment, we disrupted sterol-rich regions by application of the sterol-depleting reagent methyl-β-D-cyclodextrin (MCD). Sterol depletion affected more than half of the analyzed Triton X-100 DRM proteins. These proteins are suggested to likely be "core" lipid domain proteins (Dataset S1). Forty-one proteins were no longer detected after MCD treatment, the majority being signaling proteins (41.5%) like leucine-rich-repeat (LRR)-like protein kinases and the calcium-dependent protein kinases CPK10 and -21.

Stimulated Emission-Depletion Measurements of Membrane Domain Size. To verify their membrane domain association, we found that microscopic visualization of the respective proteins within the PM was effective. In all plant proteomic studies on PM DRMs, including ours, members of the remorin protein family were detected. Up to now, knowledge of biological function of remorin proteins has been limited, and there are only few examples in which the biological function could be revealed to some extent (27, 28). We therefore assessed the size of the remorin patches with the help of stable transgenic *Arabidopsis* eGFP::StRem1.3 plants and STED (stimulated emission-depletion) microscopy to obtain super-resolution, background- and artifact-free images (29). STED microscopy considerably improved the resolution of the images compared with conventional confocal microscopy (Fig. 1 *A*–*E*). The size of the fluorescently labeled structures could be narrowed down to ~97 nm (Fig. 1 *C* and *E*, black striped bars), well in line with measurements of a "lipid raft" diameter being below 100 nm in animal cells. Complementary analysis of these structures with classic confocal microscopy reveals a mean membrane domain diameter of 250 nm (Fig. 1 *B*, *D*, and *E*, gray striped bars), suggesting that analysis by confocal microscopy might result in misleading measurements of membrane micro- or nanodomain size.

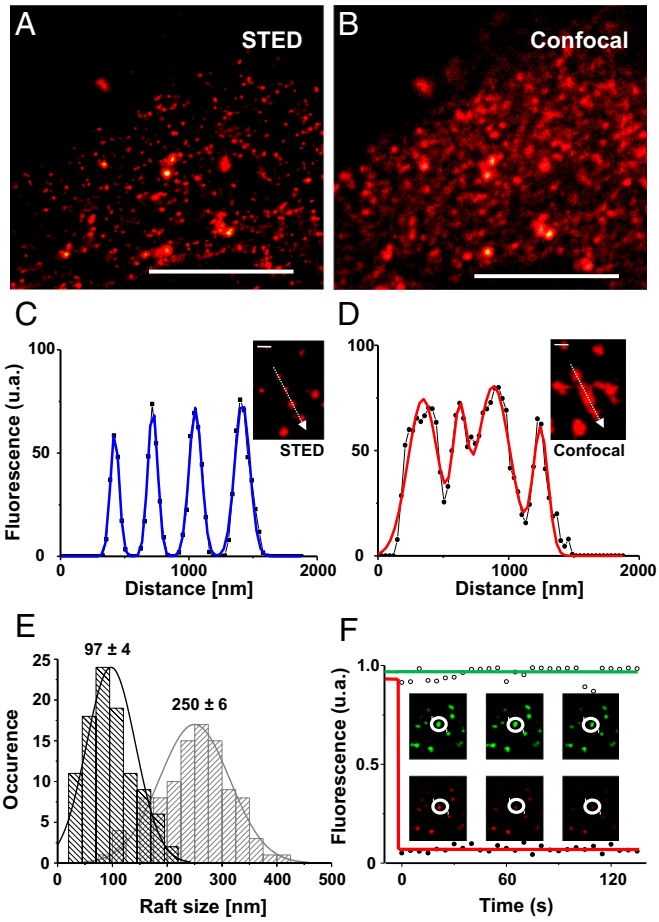

Fig. 1. STED characterization of *A. thaliana* eGFP::StRem 1.3 overexpressor lines and lateral mobility determination of DsRed2::AtRem 1.3. Images (*A*–*D*) and line measurements of identical regions with confocal microscopy (*B* and *D*) and STED (*A* and *C*) reveal much better resolution of STED microscopy. The data were fit to Gaussians in *C* and *D*. (Scale bars, 10 μm in *A* and *B*, 250 nm in *C* and *D*.) (*E*) StREm 1.3 spot size distribution of same spots ($n > 100$) as determined with STED (black hatched bars, mean 97 ± 4 nm) or with confocal microscopy (gray hatched bars, mean 250 ± 6 nm). (*F*) FRAP measurements illustrate almost no lateral mobility (recovery) of DsRed2::AtRem 1.3 (red graph and *Lower Insets*) normalized to a nonphotobleached but colocalized eGFP::AtRem 1.2 (green graph and *Upper Insets*). The bleach and control spots are circled.

***Arabidopsis Thaliana* Remorins 1.2/1.3 (AtRem 1.2/1.3) as Membrane Domain Markers.** In *A. thaliana*, 16 remorin genes were identified and classified into six different groups based on genomic data (30). *Arabidopsis Thaliana* remorins (AtRem) 1.2 and 1.3 were identified as constant sterol-dependent constituents of *Arabidopsis* PM DRMs (31–33). Confocal analysis of *Arabidopsis* epidermal cells transiently expressing GFP- or DsRed-labeled AtRem 1.2 and 1.3 fusion proteins revealed a spotted pattern of remorin distribution within the PM (Fig. S1). AtRem 1.2 and AtRem 1.3 showed an excellent colocalization (Pearson's and Spearman's correlation of 0.728 ± 0.042 and 0.629 ± 0.054). Furthermore, AtRem 1.3 clearly colocalized with the accepted plant membrane domain marker StRem 1.3 (27) after transient expression in *A. thaliana* epidermal cells (Fig. 2 *A*–*D*). Fluorescence recovery after photobleaching (FRAP) experiments revealed almost no photorecovery of DsRed2::AtRem 1.3 after photobleaching (Fig. 1*F*), indicating low mobility of the protein within the PM. We therefore used AtRem 1.2 and 1.3 as marker proteins to characterize *Arabidopsis* PM domains in detail in vivo and will refer to StRem 1.3 and AtRem 1.3-marked membrane domains as "stable nanodomains" owing to their size and immobility. To investigate whether the "patchy" localization of remorin proteins depends on the sterol composition of the PM, stable *A. thaliana* lines expressing eGFP::StRem 1.3 (Fig. 2 *E* and *F*) were used to isolate DRMs. In accordance with the initial proteomic data, Western blot and mass spectrometric analyses showed that treatment with the sterol-depleting agent MCD significantly shifted the abundance of eGFP::StRem 1.3 from DRMs to the detergent-soluble fraction (DSF; Fig. 2 *G* and *H* and Dataset S2; raw files and search results can be accessed under the dataset identifier PXD000182 at the ProteomeXchange database and PRIDE, http://proteomecentral.proteomexchange.org/). This finding was consistent with previous reports from quantitative proteomic analyses that investigated the effects of sterol-depleting agents in *A. thaliana* cell culture (31).

CPK21 and SLAH3 Interact in DRMs. Recently the SLAC/SLAH family of anion channels was identified (34, 35). SLAC1, the founder of this family, represents a guard cell S-type anion channel regulated by ABI1 and CPK21/23 in an ABA- and Ca^{2+}-dependent manner (14). The activity of CPK21 seems to be regulated by the

PLANT BIOLOGY

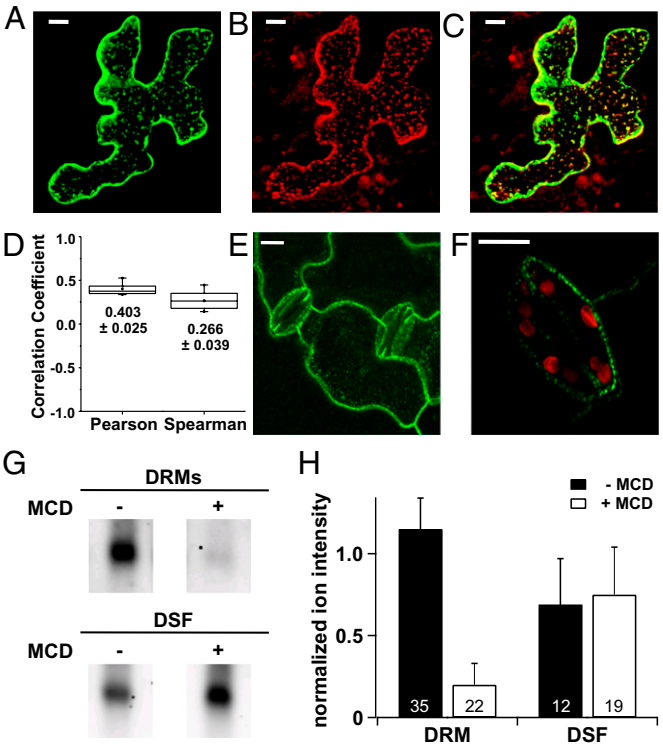

Fig. 2. Colocalization of DsRed2::AtRem 1.3 with eGFP::StRem 1.3 in an *Arabidopsis* overexpressor line. (*A*) eGFP::StRem 1.3, (*B*) DsRed2::AtRem 1.3, merge in *C*. (*D*) Statistical analysis revealed a clear colocalization of DsRed2::AtRem 1.3 and eGFP::StRem 1.3 (n = 7, average ± SE). (*E* and *F*) "Patchy" appearance of eGFP::StRem 1.3 in stomatal guard cells and epidermal cells. (Scale bars, 10 μm.) (*G*) Western blot analysis of DRMs isolated from stable eGFP::StRem 1.3 expressing plants with or without MCD sterol depletion. eGFP::StRem 1.3 dissociated from DRMs upon MCD treatment and was detected in the DSF (protein input = 15 μg). (*H*) Normalized and scaled ion intensities of StREM1.3 in DRM and DSF fractions with and without MCD treatment. Significant differences between treatments was tested by one-way ANOVA using cRacker (ANOVA P = 0.032717). Numbers indicate the number of identified and quantified peptides for each treatment.

complex between the protein phosphatase 2C (PP2C) ABI1 and an ABA receptor of the RCAR/PYR/PYL family. Although SLAC1 is exclusively expressed in guard cells (34), one of its homologs, SLAH3, is expressed in *Arabidopsis* mesophyll cells as well (12). Because SLAH3 was not yet detected in proteomic approaches (36, 37), we aimed to overcome the low signal density of a rare PM channel protein by transient overexpression. Using *Nicotiana benthamiana* leaves and *Agrobacterium tumefaciens*-mediated transfection, we expressed ABI1, CPK21, and SLAH3 fused to appropriate detection tags in epidermal cells and isolated DRMs from these leaves. Label-free mass spectrometry-based peptide quantitation and Western blot analysis revealed the presence of CPK21 both in DRM and DSF (Fig. 3 *A* and *C*, Fig. S2*A*, and Dataset S3; raw files and search results can be accessed under the dataset identifier PXD000182 at the ProteomeXchange database and PRIDE, http://proteomecentral.proteomexchange.org/). Immunologic investigation of CPK21 localization in DRMs after MCD treatment uncovered a strong sterol dependency, which also supports the mass spectrometric data (Fig. S2*A*).

In contrast to CPK21, SLAH3 alone was found to be more abundant in the detergent-soluble fraction (Fig. 3 *B* and *C* and Dataset S3). Coexpression of CPK21 and SLAH3, however, clearly directed both proteins into the DRM fraction (Fig. 3, Fig. S2*B*, and Dataset S3). On the other hand, additional coexpression of ABI1 to the DRM-localized CPK21/SLAH3 complex led to a shift of both CPK21 and SLAH3 from DRMs into the DSF (Fig. 3, Fig. S2*B*, and Dataset S3). Therefore, the PP2C ABI1 seems to displace both the kinase CPK21 and the ion channel SLAH3 from the postulated lipid cluster to the detergent-soluble fraction.

To visualize the physical interaction of the aforementioned ABA signaling components, we took advantage of the bimolecular fluorescence complementation technique [BiFC (38)]. ABI1, CPK21, and SLAH3 were fused to complementary halves of split YFP and transferred into *A. thaliana* epidermal cells by ballistic bombardment. Subsequent analysis by confocal microscopy revealed the physical interaction of CPK21::YFP^N (CPK21 fused to the N-terminal half of YFP) and SLAH3::YFP^C (SLAH3 fused to the C-terminal half of YFP; see ref. 12; Fig. 4*A*). BiFC fluorescence was also detectable in cells transformed with ABI1::YFP^C and CPK21::YFP^N (Fig. 4*E*). Interestingly, the BiFC signal was always restricted to membrane spots resembling those visible after AtRem 1.3 expression. Consequently, we analyzed whether the protein pairs SLAH3/CPK21 and CPK21/ABI1 were colocalized with the nanodomain marker protein AtRem 1.3 (Fig. 4 *B* and *C* and 4 *F* and *G*, respectively). Pearson's and Spearman's correlation ranks indicated a very good colocalization (Fig. 4 *D* and *H*). From this finding we concluded that the Ca^{2+}-dependent kinase CPK21 interacts with SLAH3 as well as with the ABA signaling protein phosphatase PP2C ABI1 within AtRem1.3-labeled nanodomains.

Electrophysiological Characterization of CPK21–SLAH3 Interaction. To further investigate whether localization of the putative ABA signaling complex ABI1/CPK21/SLAH3 in membrane nanodomains

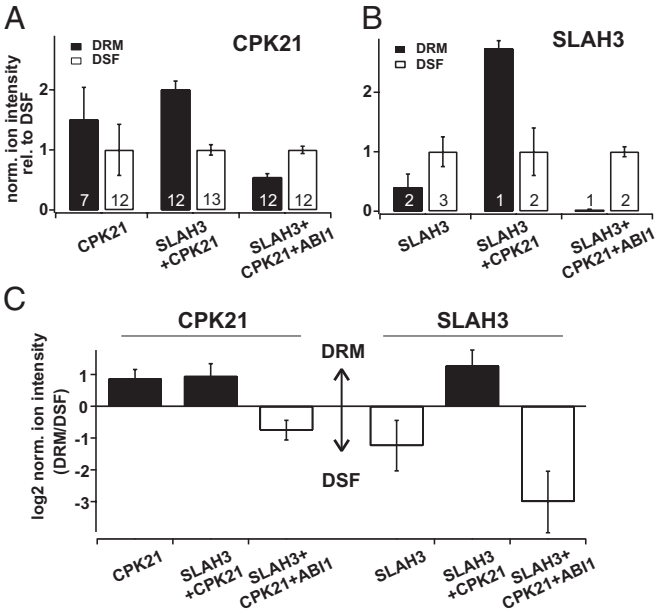

Fig. 3. ABI1-dependent CPK21-SLAH3 colocalization in DRMs. Presence of ABI1 released both CPK21 and SLAH3 from DRMs and led to transition into the DSF. Normalized and scaled ion intensities of (*A*) CPK21::YFP and (*B*) SLAH3::V5 expressed in *N. benthamiana* in combinations with and without ABI1. From each plant expressing combinations of constructs, two to three biological replicates were analyzed and averaged. To avoid influences from different protein expression levels for different construct combinations and replicates, the DSF intensity was set to 1 and the DRM signal was calculated accordingly. Significant differences were tested by ANOVA using cRacker (51). (*C*) For each combination of constructs expressed in *N. benthamiana*, the DRM/DSF ratio was calculated from normalized ion intensities and averaged between biological replicates. Black bars indicate higher protein abundance in DRM fraction, and white bars indicate higher abundance in the DSF. Error bars represent SDs as calculated from two to three biological replicates. Numbers depict the number of identified and quantified peptides for each treatment.

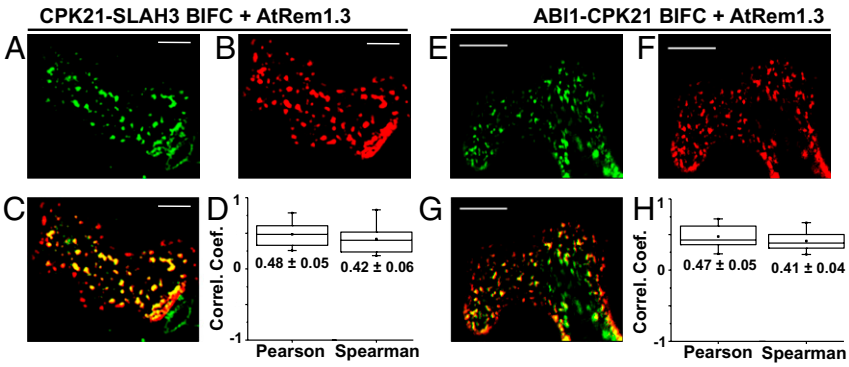

Fig. 4. CPK21-SLAH3 and ABI1-CPK21 interaction in membrane domains. BiFC interaction between CPK21::YFP^N and SLAH3::YFP^C (*A–D*) or ABI1::YFP^C and CPK21::YFP^N (*E–H*) and colocalization with DsRed::AtRem 1.3. (*A*) BiFC SLAH3-CPK21, (*B*) DsRed::AtRem 1.3, (*C*) merge, (*D*) statistical analysis of colocalization: Pearson's and Spearman's correlation factors >0 indicated a tendency toward colocalization (n = 13, ±SE). (*E*) BiFC ABI1-CPK21, (*F*) DsRed::AtRem 1.3, (*G*) merge, (*H*) statistical analysis of colocalization (n = 11, ±SE). (Scale bars, 10 μm.)

is necessary for channel function, we heterologously expressed the signaling components in *Xenopus laevis* oocytes. Coexpression of SLAH3::YFP^C and CPK21::YFP^N resulted in spotted fluorescent structures in the oocyte PM (Fig. S3*A*). When coexpressed with eGFP::AtRem 1.3 cRNA, the CPK21/SLAH3-BiFC signal correlated with AtRem 1.3-labeled membrane domains (Fig. S3 *B–D*). In analogy to the situation in *Arabidopsis* epidermal cells, the CPK21/SLAH3 signaling complex seems to be located in distinct membrane domains in oocytes as well. To test whether nanodomain localization of SLAH3 is influenced by the protein phosphatase ABI1, we coinjected *Xenopus* oocytes with SLAH3::YFP^C and CPK21::YFP^N cRNA in the absence and presence of ABI1 cRNA. In agreement with the observed removal of the CPK21/SLAH3 complex from nanodomains in the presence of ABI1 in plant cells, fluorescent CPK21/SLAH3-BiFC spots were also detected to a much lesser extent in the ABI1-coinjected oocytes (Fig. S4). This suggests that the presence of ABI1 indeed prevents the interaction of CPK21 and SLAH3 in distinct membrane domains.

To test whether SLAH3 function is affected by its localization, we monitored SLAH3-mediated oocyte anion currents. Notably, coexpression of SLAH3 with CPK21 resulted in pronounced (μA) S-type anion currents (Fig. 5*B*) (12). In oocytes injected with AtRem1.3 only, no currents were observed (Fig. 5*A*). Expression of AtRem 1.3 together with CPK21/SLAH3 did not alter SLAH3-mediated anion currents (Fig. 5 *C* and *D*), indicating that AtRem 1.3 does not function as an ion channel regulator. Corresponding to the disappearance of CPK21/SLAH3 interaction in defined membrane domains upon coexpression with ABI1 (Fig. S4), SLAH3 activation by CPK21 was abolished in the presence of ABI1 (Fig. 5 *E* and *F*). Thus, CPK21–SLAH3 interaction within specific membrane domains seems to be necessary for SLAH3-mediated anion transport, and ABI1 might inhibit the formation of the active CPK21/SLAH3 signaling complex at the oocyte PM.

Modulation of SLAH3–CPK21 Interaction by ABA. Because ABI1 overexpression does not necessarily mimic changes in endogenous ABA levels, we aimed to verify that the interaction between SLAH3 and its activating kinase, CPK21, is not only affected by absence or presence of overexpressed ABI1 in the respective cell type but directly depends on the phytohormone ABA. We therefore further specified the interaction studies with the help of the acceptor bleaching Förster resonance energy transfer technique (AB-FRET) (39–42). FRET efficiency in *A. thaliana* protoplasts transiently expressing SLAH3::CFP and CPK21::YFP was significantly enhanced upon the application of ABA, indicating an increase in physical interaction between SLAH3 and CPK21 (Fig. S5*A*). As expected, this ABA-dependent increase in FRET interaction between the anion channel and its activating kinase was most pronounced at the PM of the observed protoplast system (Fig. S5*B*). In accordance with our previous results, coexpression of ABI1 prevented the ABA-induced increase in physical interaction between SLAH3 and CPK21. Additional coexpression of the ABA-receptor RCAR1/PYL9 abolished inhibition by ABI1, and we could again

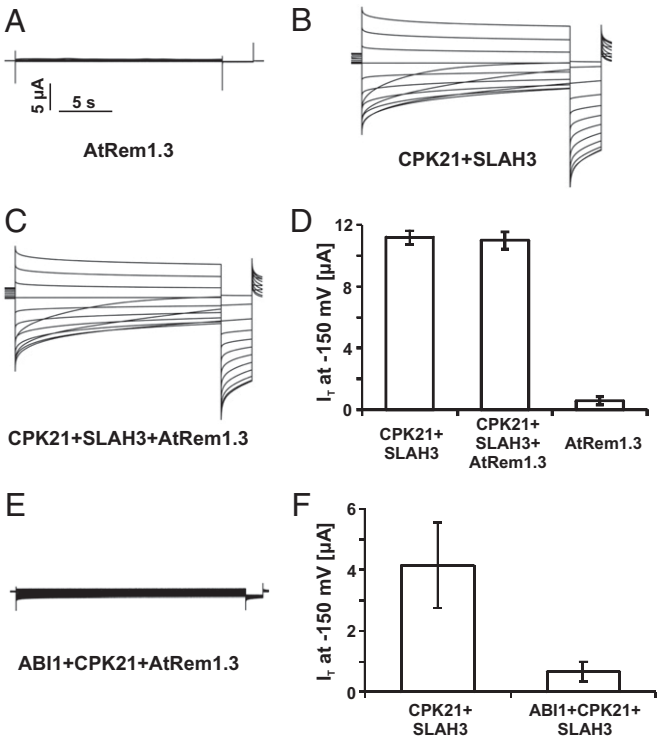

Fig. 5. Electrophysiological characterization of ABI1-CPK21-SLAH3 interaction in *X. laevis* oocytes. (*A–C*) Characteristic whole-oocyte currents in response to 20-s single voltage pulses ranging from +40 to −60 mV for (*A*) AtRem 1.3, (*B*) CPK21::YFP^N + SLAH3::YFP^C, and (*C*) AtRem 1.3 + CPK21::YFP^N + SLAH3::YFP^C. (*D*) AtRem 1.3 did not alter the electrophysiological characteristics of CPK21-activated SLAH3. Instantaneous currents were recorded at −150 mV: AtRem 1.3 and SLAH3 expression induced no currents until the protein kinase CPK21 was additionally expressed. CPK21 application activated SLAH3 S-type anion currents (mean ± SD, n = 4). (*E* and *F*) Additional coexpression of the protein phosphatase ABI1 prevented SLAH3 activation by CPK21 (*E*, conditions identical to measurements in *A–C*). Nitrate-induced currents were significantly reduced by ABI1 injection (*F*) in the presence of 10 mM NO_3^- (mean ± SD, n = 7 for CPK21 + SLAH3 and n = 4 for ABI1 + CPK21 + SLAH3).

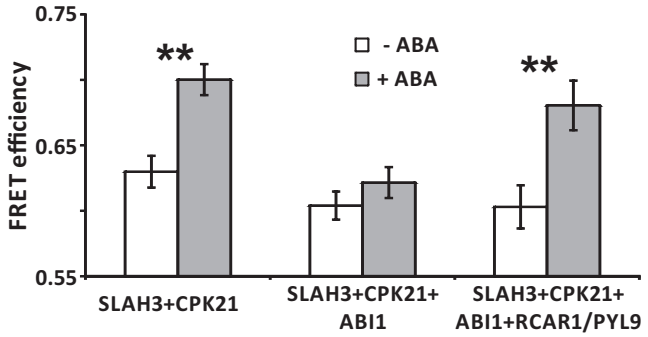

Fig. 6. ABA-induced interaction between SLAH3 and CPK21 is modulated by ABI1 and RCAR1/PYL9. Treatment of *Arabidopsis* protoplasts transiently expressing CPK21::YFP and SLAH3::CFP with 50 μM ABA led to an increase in FRET efficiency after acceptor photobleaching. Whole protoplasts were bleached and therefore defined as region of interest ($n = 90$, average ± SE). Additional expression of ABI1::mCherry prevented the ABA-induced increase in FRET efficiency ($n = 70$, average ± SE). Coexpression of the ABA receptor RCAR1/PYL9::mEos prevented ABI1-mediated inhibition and the ABA-induced increase in FRET efficiency between SLAH3::CFP and CPK21::YFP was detected ($n = 20$, average ± SE).

observe the ABA-stimulated increase in physical SLAH3/CPK21 interaction (Fig. 6). We therefore propose that ectopically expressed RCAR1/PYL9 was able to compensate for ABI1 overexpression by binding to the phosphatase leading to ABI1 inhibition. As a result, CPK21 was relieved from ABI1 suppression, which allowed FRET interaction in an ABA-dependent manner.

Discussion

Using different detergents and digestion protocols, we were able to classify 120 proteins as putative membrane nanodomain residents that were not described in previous proteomic studies on plant DRMs (24, 25, 31–33, 43). Two proteins of yet unknown function in *Arabidopsis*, AtRem 1.2 and 1.3, were found to depend on a sterol-rich environment, suggesting their preferential localization within membrane nanodomains. MCD sensitivity and colocalization of transiently expressed DsRed2::AtRem 1.3 with the well-accepted plant membrane domain marker from potato [eGFP::StRem 1.3 (27)] in small essentially immobile membrane structures (diameter <100 nm) make AtRem 1.3 an indicator for sterol-rich lipid environments in *Arabidopsis*.

More than 40% of all identified DRM proteins in this study are involved in signaling and transport, suggesting that distinct plant PM domains act as association platforms for signaling and transport processes. Among the 66 proteins that were negatively affected by treatment with MCD, we found a remarkably large number of protein kinases, and sterol dependence of CPK21 especially caught our attention. CPKs play key roles in ABA/drought stress signaling, translating elevated Ca^{2+} levels to channel activation and gene transcription (12, 14, 44). Fast ABA-induced stomatal closure has been shown to essentially depend on the guard cell anion channels SLAC1 and SLAH3. Thereby, SLAC1 is activated by OST1/CPK23 in a calcium-independent and by CPK21 in a calcium-dependent manner. In contrast, SLAH3 is predominantly phosphorylated and activated by CPK21 (12–14). Both protein kinases are controlled by the protein phosphatase ABI1 via the ABA receptor RCAR1/PYL9. Here we showed that a fraction of this signaling phosphatase is associated with PM nanodomains in mesophyll cells, controlling anion conductance via the CPK21/SLAH3 complex. In the presence of ABA, owing to inhibition of the phosphatase ABI1, CPK21 phosphorylates the N terminus of SLAH3, turning the channel into an anion-conducting mode (12). We could demonstrate that in *Arabidopsis* mesophyll cells, all ABA signaling components regulating membrane-delimited steps downstream of the central PP2C ABI1 are at least transitionally associated with stable AtRem 1.3 lipid nanodomains. Particularly, CPK21 and SLAH3 seem to predominantly interact in such membrane domains, which results in channel activation and anion efflux. In the presence of ABI1, SLAH3 and CPK21 do not enter common lipid nanodomains. This inhibits the interaction between the anion channel and its activating kinase and thus prevents SLAH3-mediated anion currents. We were able to demonstrate that the interaction between SLAH3 and CPK21 is directly modulated by the phytohormone ABA in *Arabidopsis* protoplasts and that this modulation is affected by ABI1 and the ABA receptor RCAR1/PYL9 (cf. 45 for ABA-dependent gene regulation in protoplast assays). We therefore suggest that the phytohormone ABA affects SLAH3 function by controlling membrane localization of the anion channel and its activating kinase via inhibition of ABI1. In other plant cell types or yeast, the localization of transport proteins within membrane domains was also shown to influence their activity (46, 47). In the animal field, the membrane domain concept has recently shifted to a more dynamic view. It has been proposed that the composition of membrane domains may vary, ranging from short-lived nanoscale assemblies to more stable domains with variable size and lifetime (17). Stimulus-induced alterations in domain composition could be explained by two mechanisms: (*i*) aggregation of nanoscale domains to larger platforms (and subsequent diffusion), or (*ii*) association/dissociation of proteins to/from preexisting microdomain environments. For the plant field, the second mechanism has been favored (48), and our data may support this view. However, we cannot exclude that there are different subsets of membrane domains in plants as well with only a part of them being occupied by remorin proteins or the described ABA signaling components.

In this study, we could demonstrate the existence of a functional signaling complex in plant membrane nanodomains. The interaction of CPK21 and SLAH3 within common membrane domains is required for SLAH3-mediated anion transport, whereas the phosphatase ABI1 blocks the formation of the CPK21/SLAH3 signaling complex at the PM in an ABA-dependent manner.

Materials and Methods

Preparation of DRMs. PM vesicles were prepared from *A. thaliana* leaves or from *N. benthamiana* leaves by aqueous two-phase partitioning (detailed information concerning growth conditions, transformation of *N. benthamiana*, and PM purification procedure is provided in *SI Materials and Methods*). Sterols were depleted using 25 mM methyl-β-D-cyclodextrin. Sterol-depleted and nontreated PM were subjected to isolation of DRMs with 1% (vol/vol) Triton X-100 or Brij-98 (*SI Materials and Methods*). DRM samples were then subjected to SDS/PAGE and Western blotting or MS analysis. Antibodies are described in *SI Materials and Methods*.

MS Analysis of DRM Fractions. DRM proteins were separated on continuous gradient polyacrylamide and digested with trypsin. Alternatively, dried DRMs were solubilized in 60% (vol/vol) DMSO and then subjected to trypsin digestion. The obtained peptide mixtures were preconcentrated and separated using an Ultimate 3000 nano-HPLC system (Dionex). An LCQ DecaXPPlus ion trap mass spectrometer (ThermoElectron) repeatedly acquired one full-MS and three tandem-MS spectra from the nano-HPLC separated samples; or a Quad-TOF QSTAR XL (Applied Biosystems) acquired one full-MS and two tandem-MS spectra. The tandem-MS spectra were searched against the TAIR v9 protein database using the MascotDaemon and the Mascot algorithm. Detailed information is provided in *SI Materials and Methods*.

Label-Free Peptide Quantitation. DRM proteins were predigested in solution using Lys C, followed by trypsin digestion. Tryptic peptide mixtures were analyzed by LC/MS/MS using nanoflow HPLC (Proxeon Biosystems) and an orbitrap (LTQ-Orbitrap; Thermo Scientific) as mass analyzer. Protein identification and ion intensity quantitation was carried out by MaxQuant version 1.3.0.5 (49). Spectra were matched against the *Arabidopsis* proteome (TAIR10, 35,386 entries) using Andromeda (50). Quantitative statistical analysis of protein abundances in the different fractions was carried out using cRacker (51). Detailed information is provided in *SI Materials and Methods*.

Confocal Fluorescence Microscopy. *A. thaliana* leaves were transiently transformed by ballistic bombardment, and fluorescent images of transformed cells were obtained using confocal microscopes (LSM5 Pascal, Carl Zeiss Microimaging; or TCS SP5, Leica). STED images were acquired on a Leica SP5 STED microscope using immunohistochemically stained leaves of a stable *A. thaliana* eGFP::StRem 1.3 line. Further information is provided in *SI Materials and Methods*.

Oocyte Recordings. Oocyte preparation and cRNA generation and injection have been described elsewhere (14). In two-electrode voltage-clamp studies oocytes after 2 or 3 d of expression were perfused with Kulori-based solutions. Detailed information is provided in *SI Materials and Methods*. For documentation of the oocyte BiFC results, pictures were taken with a confocal laser scanning microscope (LSM 5 Pascal; Carl Zeiss) equipped with a Zeiss Plan-Neofluar 20×/0.5 objective. Detailed information is provided in *SI Materials and Methods*.

ACKNOWLEDGMENTS. We thank S. Mongrand (University of Bordeaux) for kind donation of a StRem1.3 vector construct. This work was funded by the DFG (German Science Foundation) Graduiertenkolleg 1342 (F.D., C.H., J.O.B., S.S., Y.R., D.G., G.S.H., I.K., and R.H.), by DFG grants within Forschergruppe 964 (to R.H.), by the DFG Center for Excellence in Biomedicine FZ-82 (G.S.H.), by the Bavarian Ministry for Research and Education for the Bio-Imaging Center at the University of Würzburg (J.O.B. and G.S.H.), and by a Howard Hughes Medical Institute grant (to G.S.H.). The mass spectrometry proteomics data have been deposited in the ProteomeXchange Consortium (http://proteomecentral.proteomexchange.org/) via the PRIDE partner repository (52) with the dataset identifier PXD000211 and DOI 10.6019/PXD000211 for Dataset S1 and PXD000182 for Datasets S2 and S3.

1. Leonhardt N, et al. (2004) Microarray expression analyses of *Arabidopsis* guard cells and isolation of a recessive abscisic acid hypersensitive protein phosphatase 2C mutant. *Plant Cell* 16(3):596–615.
2. Seki M, Umezawa T, Urano K, Shinozaki K (2007) Regulatory metabolic networks in drought stress responses. *Curr Opin Plant Biol* 10(3):296–302.
3. Seki M, et al. (2002) Monitoring the expression pattern of around 7,000 *Arabidopsis* genes under ABA treatments using a full-length cDNA microarray. *Funct Integr Genomics* 2(6):282–291.
4. Yang Z (2008) Cell polarity signaling in *Arabidopsis*. *Annu Rev Cell Dev Biol* 24: 551–575.
5. Wang RS, et al. (2011) Common and unique elements of the ABA-regulated transcriptome of *Arabidopsis* guard cells. *BMC Genomics* 12:216.
6. Fujii H, et al. (2009) In vitro reconstitution of an abscisic acid signalling pathway. *Nature* 462(7273):660–664.
7. Ma Y, et al. (2009) Regulators of PP2C phosphatase activity function as abscisic acid sensors. *Science* 324(5930):1064–1068.
8. Park SY, et al. (2009) Abscisic acid inhibits type 2C protein phosphatases via the PYR/PYL family of START proteins. *Science* 324(5930):1068–1071.
9. Furihata T, et al. (2006) Abscisic acid-dependent multisite phosphorylation regulates the activity of a transcription activator AREB1. *Proc Natl Acad Sci USA* 103(6): 1988–1993.
10. Brault M, et al. (2004) Plasma membrane depolarization induced by abscisic acid in *Arabidopsis* suspension cells involves reduction of proton pumping in addition to anion channel activation, which are both Ca2+ dependent. *Plant Physiol* 135(1): 231–243.
11. Trouverie J, et al. (2008) Anion channel activation and proton pumping inhibition involved in the plasma membrane depolarization induced by ABA in *Arabidopsis thaliana* suspension cells are both ROS dependent. *Plant Cell Physiol* 49(10): 1495–1507.
12. Geiger D, et al. (2011) Stomatal closure by fast abscisic acid signaling is mediated by the guard cell anion channel SLAH3 and the receptor RCAR1. *Sci Signal* 4(173):ra32.
13. Geiger D, et al. (2009) Activity of guard cell anion channel SLAC1 is controlled by drought-stress signaling kinase-phosphatase pair. *Proc Natl Acad Sci USA* 106(50): 21425–21430.
14. Geiger D, et al. (2010) Guard cell anion channel SLAC1 is regulated by CDPK protein kinases with distinct Ca^{2+} affinities. *Proc Natl Acad Sci USA* 107(17):8023–8028.
15. Brandt B, et al. (2012) Reconstitution of abscisic acid activation of SLAC1 anion channel by CPK6 and OST1 kinases and branched ABI1 PP2C phosphatase action. *Proc Natl Acad Sci USA* 109(26):10593–10598.
16. Foster LJ, De Hoog CL, Mann M (2003) Unbiased quantitative proteomics of lipid rafts reveals high specificity for signaling factors. *Proc Natl Acad Sci USA* 100(10): 5813–5818.
17. Simons K, Gerl MJ (2010) Revitalizing membrane rafts: New tools and insights. *Nat Rev Mol Cell Biol* 11(10):688–699.
18. Zappel NF, Panstruga R (2008) Heterogeneity and lateral compartmentalization of plant plasma membranes. *Curr Opin Plant Biol* 11(6):632–640.
19. Malinsky J, Opekarová M, Tanner W (2010) The lateral compartmentation of the yeast plasma membrane. *Yeast* 27(8):473–478.
20. London E, Brown DA (2000) Insolubility of lipids in triton X-100: Physical origin and relationship to sphingolipid/cholesterol membrane domains (rafts). *Biochim Biophys Acta* 1508(1-2):182–195.
21. Lingwood D, Simons K (2007) Detergent resistance as a tool in membrane research. *Nat Protoc* 2(9):2159–2165.
22. Shogomori H, Brown DA (2003) Use of detergents to study membrane rafts: The good, the bad, and the ugly. *Biol Chem* 384(9):1259–1263.
23. Peskan T, Westermann M, Oelmuller R (2000) Identification of low-density Triton X-100-insoluble plasma membrane microdomains in higher plants. *Eur J Biochem* 267(24):6989–6995.
24. Shahollari BP-BTOR (2004) Receptor kinases with leucine-rich repeats are enriched in Triton X-100 insoluble plasma membrane microdomains from plants. *Physiol Plant* 122:397–403.
25. Mongrand S, et al. (2004) Lipid rafts in higher plant cells: Purification and characterization of Triton X-100-insoluble microdomains from tobacco plasma membrane. *J Biol Chem* 279(35):36277–36286.
26. Tanner W, Malinsky J, Opekarová M (2011) In plant and animal cells, detergent-resistant membranes do not define functional membrane rafts. *Plant Cell* 23(4):1191–1193.
27. Raffaele S, et al. (2009) Remorin, a solanaceae protein resident in membrane rafts and plasmodesmata, impairs potato virus X movement. *Plant Cell* 21(5):1541–1555.
28. Lefebvre B, et al. (2010) A remorin protein interacts with symbiotic receptors and regulates bacterial infection. *Proc Natl Acad Sci USA* 107(5):2343–2348.
29. Klar TA, Jakobs S, Dyba M, Egner A, Hell SW (2000) Fluorescence microscopy with diffraction resolution barrier broken by stimulated emission. *Proc Natl Acad Sci USA* 97(15):8206–8210.
30. Raffaele S, Mongrand S, Gamas P, Niebel A, Ott T (2007) Genome-wide annotation of remorins, a plant-specific protein family: Evolutionary and functional perspectives. *Plant Physiol* 145(3):593–600.
31. Kierszniowska S, Seiwert B, Schulze WX (2009) Definition of *Arabidopsis* sterol-rich membrane microdomains by differential treatment with methyl-beta-cyclodextrin and quantitative proteomics. *Mol Cell Proteomics* 8(4):612–623.
32. Borner GH, et al. (2005) Analysis of detergent-resistant membranes in *Arabidopsis*. Evidence for plasma membrane lipid rafts. *Plant Physiol* 137(1):104–116.
33. Minami A, et al. (2009) Alterations in detergent-resistant plasma membrane microdomains in *Arabidopsis* thaliana during cold acclimation. *Plant Cell Physiol* 50(2):341–359.
34. Negi J, et al. (2008) CO2 regulator SLAC1 and its homologues are essential for anion homeostasis in plant cells. *Nature* 452(7186):483–486.
35. Vahisalu T, et al. (2008) SLAC1 is required for plant guard cell S-type anion channel function in stomatal signalling. *Nature* 452(7186):487–491.
36. Zhao Z, Stanley BA, Zhang W, Assmann SM (2010) ABA-regulated G protein signaling in *Arabidopsis* guard cells: A proteomic perspective. *J Proteome Res* 9(4):1637–1647.
37. Zhao Z, Zhang W, Stanley BA, Assmann SM (2008) Functional proteomics of *Arabidopsis thaliana* guard cells uncovers new stomatal signaling pathways. *Plant Cell* 20(12):3210–3226.
38. Hu CD, Chinenov Y, Kerppola TK (2002) Visualization of interactions among bZIP and Rel family proteins in living cells using bimolecular fluorescence complementation. *Mol Cell* 9(4):789–798.
39. Kenworthy AK (2001) Imaging protein-protein interactions using fluorescence resonance energy transfer microscopy. *Methods* 24(3):289–296.
40. Zhang J, Campbell RE, Ting AY, Tsien RY (2002) Creating new fluorescent probes for cell biology. *Nat Rev Mol Cell Biol* 3(12):906–918.
41. Gromova KV, Friedrich M, Noskov A, Harms GS (2007) Visualizing Smad1/4 signaling response to bone morphogenetic protein-4 activation by FRET biosensors. *Biochim Biophys Acta* 1773(12):1759–1773.
42. Vilardaga JP, Steinmeyer R, Harms GS, Lohse MJ (2005) Molecular basis of inverse agonism in a G protein-coupled receptor. *Nat Chem Biol* 1(1):25–28.
43. Morel J, et al. (2006) Proteomics of plant detergent-resistant membranes. *Mol Cell Proteomics* 5(8):1396–1411.
44. Mori IC, et al. (2006) CDPKs CPK6 and CPK3 function in ABA regulation of guard cell S-type anion- and Ca(2+)-permeable channels and stomatal closure. *PLoS Biol* 4(10): e327.
45. Moes D, Himmelbach A, Korte A, Haberer G, Grill E (2008) Nuclear localization of the mutant protein phosphatase abi1 is required for insensitivity towards ABA responses in *Arabidopsis*. *Plant J* 54(5):806–819.
46. Grossmann G, et al. (2008) Plasma membrane microdomains regulate turnover of transport proteins in yeast. *J Cell Biol* 183(6):1075–1088.
47. Li X, et al. (2011) Single-molecule analysis of PIP2;1 dynamics and partitioning reveals multiple modes of *Arabidopsis* plasma membrane aquaporin regulation. *Plant Cell* 23(10):3780–3797.
48. Simon-Plas F, Perraki A, Bayer E, Gerbeau-Pissot P, Mongrand S (2011) An update on plant membrane rafts. *Curr Opin Plant Biol* 14(6):642–649.
49. Cox J, Mann M (2008) MaxQuant enables high peptide identification rates, individualized p.p.b.-range mass accuracies and proteome-wide protein quantification. *Nat Biotechnol* 26(12):1367–1372.
50. Cox J, et al. (2011) Andromeda: A peptide search engine integrated into the MaxQuant environment. *J Proteome Res* 10(4):1794–1805.
51. Zauber H, Schulze WX (2012) Proteomics wants cRacker: Automated standardized data analysis of LC-MS derived proteomic data. *J Proteome Res* 11(11):5548–5555.
52. Vizcaino JA, et al. (2013) The Proteomics Identifications (PRIDE) database and associated tools: status in 2013. *Nucleic Acids Research* 41(D1):D1063–D1069.